# ARTICLES

## Optical Properties of Gold−Silver Iodide Nanoparticle Pair Structures

**Mahnaz El-Kouedi and Colby A. Foss, Jr.***

*Department of Chemistry, Georgetown University, Washington, D.C. 20057*

*Received: July 28, 1999; In Final Form: January 6, 2000*

Nanoparticle pair structures composed of metal (Au) and semiconductor (AgI) segments with radii ca. 16 nm have been prepared in porous anodic aluminum oxide via electrochemical template synthesis. The metal and semiconductor members can be prepared such that they are in contact or separated in the porous host. UV/visible spectra of composites in which the Au and AgI segments are in contact show a red-shifted and broadened Au particle plasmon resonance band and the absence of the AgI exciton peak normally observed at $\lambda = 425$ nm. A blue shift in the Au particle plasmon band and the reappearance of the AgI exciton peak occur as the average interparticle spacing is increased. The changes in plasmon resonance peak position are consistent with an increased probability of Au and AgI intermixing as the spacing parameter $d_{12}$ is decreased. The absence of the AgI exciton peak in the case of contacting Au and AgI particles is consistent with a large increase in the effective static dielectric constant upon phase intermixing and/or field effects associated with the contact potential at the Au/AgI interface.

### I. Introduction

The use of nanoporous media as templates for the preparation of nanoparticles composed of metal,[1−4] semiconductor,[5,6] conducting polymer,[7] and other materials is well-documented. Porous anodic aluminum oxides are particularly useful for optical studies of the nanoparticle structures prepared within their pores because the host oxide is transparent over much of the visible and infrared spectral regions. Furthermore, the parallel orientation of the cylindrical pores can lead to uniformly oriented rodlike nanostructures; polarization angle- and incidence angle-dependent optical properties can then be evaluated easily.[4,8,9]

Recently, we discussed the preparation of noncentrosymmetric gold, and gold−silver iodide nanoparticles using porous alumina-based template methods.[9,10] Noncentrosymmetric Au particle pair structures were found to produce stronger second harmonic generation signals than their centrosymmetric counterparts.[9] The linear optical properties of Au−AgI heterojunction structures were interesting vis a vis the effects of metal−semiconductor contact on the Au plasmon resonance band and the AgI exciton features.[10]

Metal−semiconductor nanoparticle structures have been prepared previously using template methods.[11] However, the large size of the metal precluded examination of particle plasmon resonance bands and the possible influence of the semiconductor phase on these bands. In our studies, we have selected alumina hosts with pores of diameter ca. 32 nm. Au segments prepared in these pores via electrodeposition give rise to strong plasmon resonance bands in the visible spectrum. AgI was chosen for the semiconductor segment because (1) its band edge (ca. 425 nm) is far removed from Au particle resonances, (2) AgI exhibits a strong exciton peak at its band edge, and (3) its electrochemical preparation in the pores of a host film is straightforward.

The optical and structural properties of AgI are well documented. At room temperature, AgI exists as two phases ($\gamma$-AgI and $\beta$-AgI) in equilibrium.[12] Berry found that the exciton peak near the band edge occurs even for AgI nanoparticles as small as 13 nm.[13] The peak is absent in particles of smaller dimensions. In a previous communication, we reported that while template-synthesized AgI nanoparticles (cylindrical radius ca. 32 nm) exhibited an exciton feature, the peak was absent when the AgI particles were prepared such that they were in contact with an Au nanoparticle segment.[10]

In this paper, we describe a template-based synthesis of Au−AgI particle structures in which the average spacing between the metal and semiconductor particle segments can be varied. We also describe the experimental UV/visible extinction spectra of these systems and compare these to the predictions of simple quasistatic limit scattering theory.

### II. Theoretical Considerations

The linear optical properties of nanoscopic particles in the UV/visible and lower energy regions of the spectrum can be described reasonably well using electrostatic expressions for particle polarizability. The so-called quasistatic limit treatment of nanoparticle optics has been reviewed extensively elsewhere, especially with regard to single particle scattering models and effective medium treatments of composite materials.[14−16] In the present context, where the optical properties of interest have been limited experimentally to arise exclusively from single particles or two interacting particles, the relevant quasistatic expression is[17,18]

* Corresponding author. E-mail: fossc@gusun.georgetown.edu. Fax: (202) 687-6209.

10.1021/jp992632h CCC: $19.00 
Published on Web 04/07/2000

$$\langle\alpha\rangle = \frac{1}{2}\frac{\alpha_1\left(1+g\frac{\alpha_2}{d_{12}^{\ 3}}\right)+\alpha_2\left(1+g\frac{\alpha_1}{d_{12}^{\ 3}}\right)}{\left(1-g^2\frac{\alpha_1\alpha_2}{d_{12}^{\ 6}}\right)} \quad (1)$$

where $\alpha_1$ and $\alpha_2$ are the polarizabilities of particles 1 and 2, and $d_{12}$ is their center to center separation distance. The factor $g$ depends on the orientation of the structure in the applied field.[18] For an electric field **E** incident along the pair axis, $g = {}^1/_2\pi$. If **E** is perpendicular to the pair axis, $g = -{}^1/_4\pi$.

Once $\langle\alpha\rangle$ is obtained as a function of incident energy, the extinction spectrum can be calculated by inserting $\langle\alpha\rangle$ into the standard expressions for $C_{ext}$.[19] Extinction spectra calculated in this manner presume that the pair structures are distributed sparsely throughout the host medium, and therefore, that electromagnetic interactions *between particle pairs* is negligible.

The average polarizability expression above provides a starting point for understanding the optical spectra of particle pairs; it addresses only the first-order dipolar interactions between the two particles[20] and not the special interfacial mixing or photochemical processes that may be operative when two materials brought into close proximity possess different electron affinities or work functions.

### III. Experimental Section

The details of the preparation of nanoporous alumina films have been described elsewhere.[8] For the present work, we prepared films ca. 50 $\mu$m in thickness which contain ca. 32 nm diameter pores. A schematic of the synthesis of Au/AgI pair structures is shown in Figure 1. Approximately 30−40 nm of silver metal was sputtered onto one face of the detached alumina film (barrier side) using an Anatech 10.2 plasma deposition device. This provided the electrical contact necessary for subsequent electrodeposition and oxidation steps. The total area of the porous alumina film subject to electrochemical modification was 3.14 cm$^2$. In the following discussion, all references to the number of coulombs (C) passed in a given synthesis step pertain to this total working electrode area. The pore area (and volume) fraction of the alumina films themselves is ca. 0.3.

An EG&G PARC model 273 potentiostat equipped with a digital coulometer was used in all electrochemical procedures. All Ag depositions were done potentiostatically at an applied voltage of −0.6 V vs a silver−silver chloride reference (SSCE). After the sputtering step, additional Ag (ca. 4 C) was then electrodeposited from a silver thiocyanate solution[21] to form the foundation for subsequent Au and Ag depositions.

Gold metal was then electrodeposited at −0.9 V vs SSCE from an Au(I) plating solution (Orotemp 24, Technic, Inc., Providence, RI). The amount of gold deposited corresponded to 0.4 or 0.5 C (vide infra). This was followed by a second layer of Ag from the thiocyanate solution. Depending on the Au−AgI particle spacing desired, three different amounts of silver (1.2, 1.275, and 1.30 C were deposited.)

To produce a structure composed of a metal (Au) and semiconductor (AgI) in close proximity, part or all of the second layer of deposited Ag is converted to AgI. The conversion to AgI was performed using a method adapted from Jaya et al.[22] After the second layer of Ag was deposited, the cell was thoroughly rinsed with deionized water, and then filled with an aqueous 0.1 M sodium perchlorate solution (prepared from analytical grade $NaClO_4$(s) purchased from Malinckdrodt). −0.6 V vs SSCE was again applied to deposit any $Ag^+$ species remaining in the alumina pores. This step is important in that it prevents the nonelectrochemical formation of AgI precipitates when the potassium iodide solution is introduced to the cell.

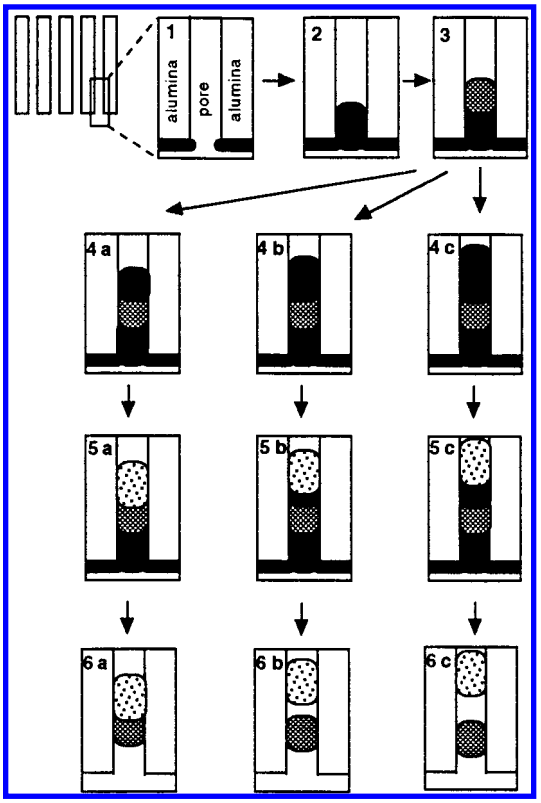


**Figure 1.** Synthesis scheme for Au/AgI pair particles. Porous alumina film is sputtered with Ag to provide electrical contact (1). Additional Ag is electrodeposited to form foundation (2). Au is electrodeposited onto Ag foundation (3). A second layer of Ag is deposited in varying amounts (4a, 4b, 4c). The second layer of Ag is converted completely (5a) or in part (5b, 5c) to AgI via electrochemical oxidation in the presence of KI solution. Nitric acid etch removes remnant Ag and leaves Au/AgI pair structures with different interparticle spacings (6a−c).

The perchlorate solution was removed and replaced with a 1 M potassium iodide solution (prepared from Fischer A.C.S grade KI solid). An equivalent of 1.2 C of the top layer of Ag was then converted to AgI via potentiostatic oxidation at 0.1 V vs SSCE. Thus, depending on the amount of Ag originally deposited, the resulting structure may be an Au particle in direct contact with AgI, or an Au particle separated from the AgI layer by a small amount of unoxidized Ag (see Figure 1). Subsequent immersion of the entire alumina composite film in concentrated nitric acid removes the Ag foundation, and any Ag left between the Au and AgI particles.

Transmission electron microscopic characterization of the Au/AgI/alumina composites was done using a JEOL 1200 EX TEM. The films samples were embedded in resin and cured overnight at 70 °C. The hardened resin was then microtomed to ca. 80 nm thick slices with a diamond knife, and placed on Cu grids (Formvar coated 200 mesh, EM Sciences) for TEM imaging. For some TEM images the nanoparticles were extracted from the oxide film using dilute nitric acid.

All spectra were taken at room temperature using a Hitachi U3501 double-beam spectrometer equipped with a model 210-2130 polarizer. In all studies at nonnormal incidence, the incident light was p-polarized. Baseline scans were defined with the polarizer and empty sample holder in the sample beam, and no material in the reference beam. During sample scans, the polarizing element was placed on the source side of the sample films. Details of the polarization spectroscopy setup can be found elsewhere.[9]

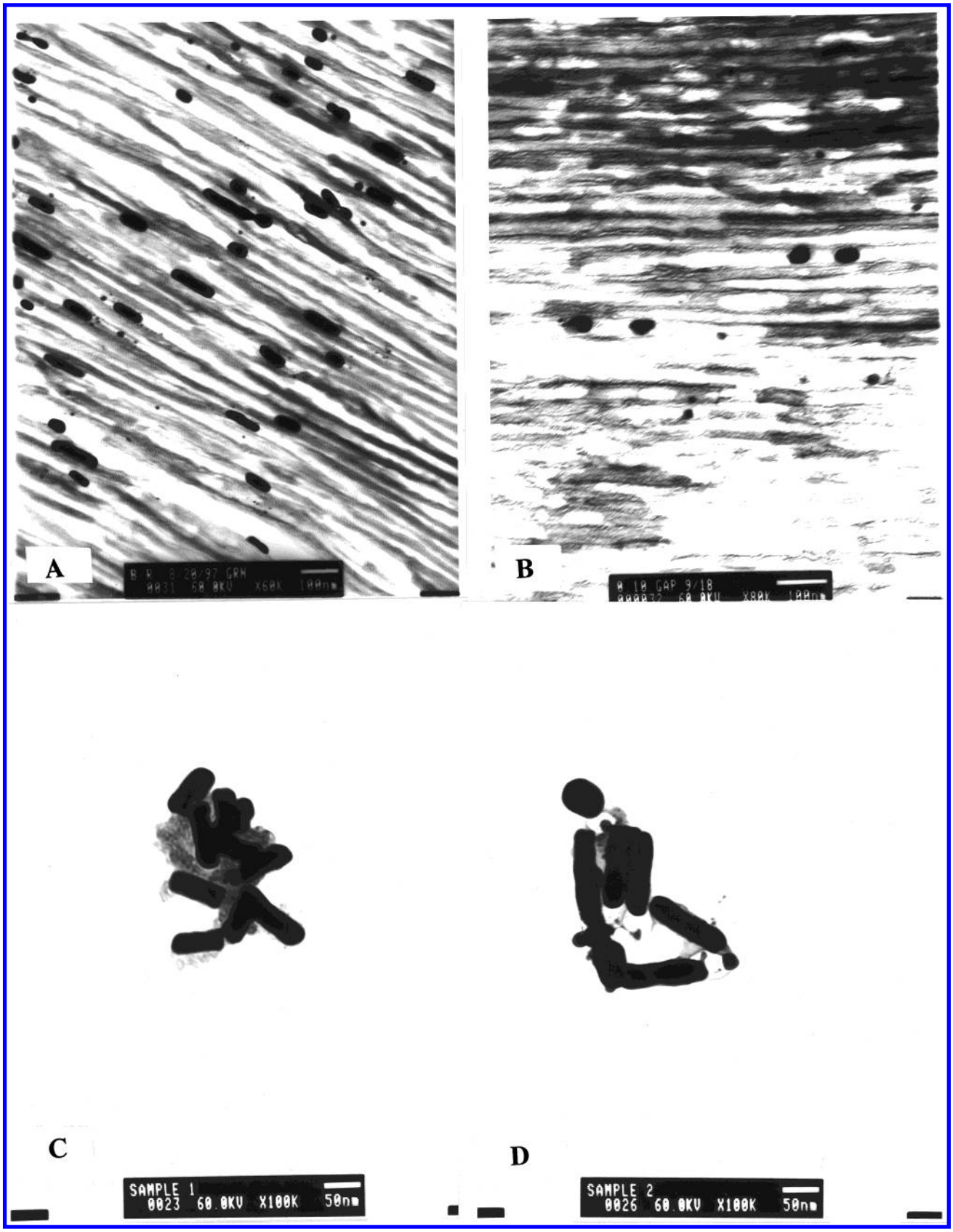


**Figure 2.** Transmission electron micrograph (TEM) images of Au/AgI particles: (A**)** Au and AgI segments in contact in aluminum oxide pores; (B**)** Au and AgI segments separated in pore after partial conversion of second Ag layer to AgI and subsequent nitric acid etch**; (**C) 0.5 C of Au-only particles extracted from oxide; (D**)** 0.5 C of Au contacting 1.2 C of AgI aslo extracted from pores using dilute sodium hydroxide solution. Scale bars in (A) and (B) denote 100 nm. Scale bars in (C) and (D) denote 50 nm.

## IV. Results and Discussion

Figure 2 shows the TEM images of Au/AgI pair nanostructures where the metal and semiconductor phases are in contact (Figure 2A) and separated by a ca. 60 nm gap (Figure 2B). The amount of Au deposited from the Au(I) plating solution was 0.4 C. The AgI layer corresponds to 1.2 C of converted Ag. As

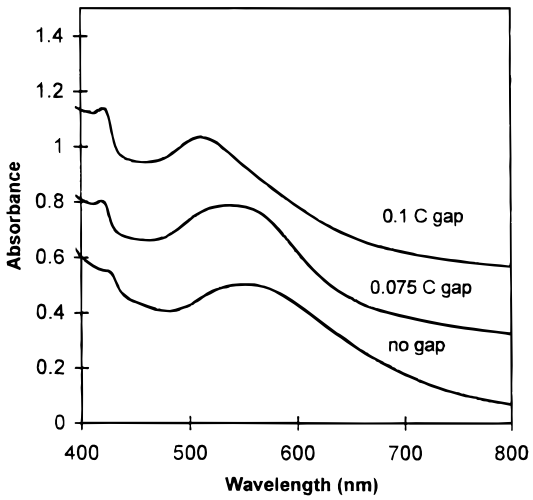


**Figure 3.** Normal incidence extinction spectra of Au (0.4 C)/AgI (1.2 C) pair structures in porous alumina films. Bottom curve: Au and AgI phases in contact. Middle curve: Au and AgI phases separated by space remaining after etching of 0.075 C Ag layer. Top curve: Au and AgI phases separated by space remaining after etching of 0.10 C Ag layer. Spectra are displaced for ease of analysis.

can be seen from Figure 2, C and D, there is no observable difference in contrast between the two phases, but there is a significant increase in length of the Au/AgI particles as compared to Au only particles. Figure 2C is a TEM image of 0.5 C Au nanoparticles extracted from the porous oxide (65 ± 2 nm). Figure 2D is 0.5 C Au in contact with 1.2C AgI (112 ± 5 nm). Samples C and D were extracted from the composite samples after they were subject to the polarization spectroscopy studies. The extraction procedure involved dissolving the alumina host in dilute sodium hydroxide and transferring the particles to a TEM grid for imaging. We find that the TEM imaging of Au/AgI pair structures is more difficult than in the case of template-synthesized gold nanoparticles[9,10] because the AgI particles are fragile and shatter during the microtoming procedure. A few intact structures can be identified, but the measurement of their dimensions and separation distances involves a larger relative error than in the case of gold nanoparticle pair structures. For the Au/AgI pair systems prepared for the examination of spacing effects, from the TEM images we estimate the gold particle members to be rods ca. 30 ± 2 nm in diameter, and 50 ± 5 nm in length. The AgI members appear to be of similar dimensions, though we note that microtome damage may favor the preservation of particles of certain dimensions and not others.

The UV/visible spectra of the Au/AgI pair structures nonetheless indicate a systematic dependence on electrochemical deposition and AgI formation conditions. Figure 3 shows the normal incidence spectra of three different composite systems. All of the spectra shown are on the same relative absorption scale. However, they have been vertically displaced for clarity. The bottom curve corresponds to the case where all of the Ag in the top deposition layer is converted to AgI. The plasmon resonance band of the Au particle is centered at ca. *555* nm, and very broad. The exciton peak normally associated with the AgI band edge at 425 nm is absent.

The upper two curves of Figure 3 correspond to composites in which the top deposition layer of Ag is only partly converted to AgI. The middle curve corresponds to the case where 1.275 C of Ag was deposited, but where only 1.20 C of Ag subsequently converted to AgI. In this system, the Au plasmon resonance band is blue-shifted to ca. 550 nm, and the AgI

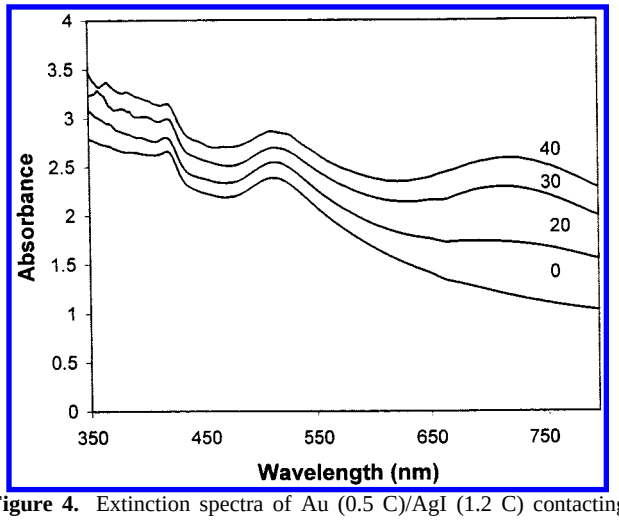


**Figure 4.** Extinction spectra of Au (0.5 C)/AgI (1.2 C) contacting pair structures in porous alumina films under p-polarization. Incidence angles shown next to curves.

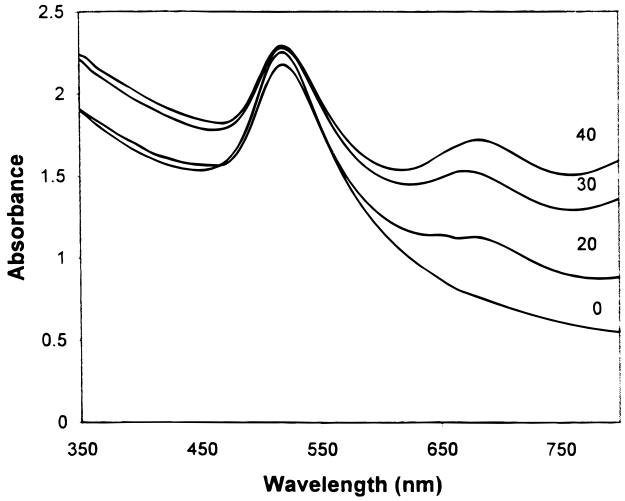


**Figure 5.** Extinction spectra of 0.5 C Au particles in porous alumina films under p-polarization. Incidence angles shown next to curves.

exciton peak is clearly visible. The composite film corresponding to the top spectrum was prepared such that 1.30 C of Ag was deposited above the Au layer, but again only 1.20 C of this Ag layer was converted to AgI. The Au plasmon resonance band peak has blue-shifted further to 517 nm and the AgI exciton peak is again apparent.

To examine further the interaction between the Au and AgI components, we conducted polarization spectroscopy studies of a pair system composed of a 1.2 C AgI segment in contact with a 0.5 C Au particle. The increased amount of deposited Au served to make the particles aspect ratios larger, and hence their plasmon resonance spectra more sensitive to incidence angle $\theta$. Figure 4 shows the UV/vis spectra of this Au/AgI system at various incidence angles under p-polarization. At normal incidence ($\theta = 0°$), there is a single asymmetric band ($\lambda_{max}$ = 530 nm), corresponding to the short-axis Au particle plasmon resonance. As $\theta$ is increased, a second very broad band (arising from the Au particle long-axis mode) appears at longer wavelength ($\lambda_{max}$ ca. 730 nm), and the AgI band edge intensity seems to diminish further.

For comparison, a composite film containing only 0.5 C Au (estimated from TEM to be ca. 65 nm in length)[8] was prepared and examined under p-polarization. Figure 5 shows the spectra of this system. The overall behavior is similar to the Au/AgI pair composite spectra shown in Figure 4. However, both the

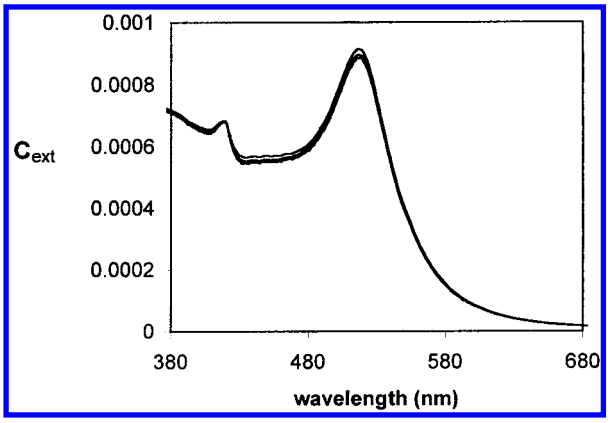


**Figure 6.** Normal incidence extinction spectra calculated using pair average polarizability model for Au/AgI nanoparticle pairs. Both Au and AgI particles are assumed to have semimajor axes **a** = 25 nm and semiminor axes **b** = 16 nm. The five spectra correspond to different center-to-center separation distances $d_{12}$ = 1 mm, 60, 53, and 50 nm (contacting particles). Overall extinction decreases with decreasing $d_{12}$.

short- and long-axis plasmon resonance bands are sharper, and the latter appears at a shorter wavelength ($\lambda_{max}$ = 690 nm).

From both the normal incidence and polarization/tilt studies, there is observed a broadening and red-shifting of the Au plasmon resonance band (either short axis or long axis) when all of the Ag phase is converted to AgI, and the final particle structure involves contact between Au and AgI phases. Spectral red shifts and damping of the plasmon resonance bands may arise from a variety of factors. One obvious factor may be Au particle size and shape distribution; for example, the electrochemical synthesis in 6a in Figure 1 may somehow lead to a larger Au particle size and shape distribution than in the case of structures 6b, which in turn would involve a greater dispersion than structure 6c. While the fragility of the structures makes it difficult to evaluate the plausibility of such an interpretation, we would note that an Au particle size distribution cannot account for the systematic trends in the AgI band edge spectra. In the following sections, we consider the effects of Au/AgI interparticle electromagnetic and phase mixing interactions.

**Comparison with Pair Average Polarizability Model**. In order to understand the observed spectral effects in Figure 3, we attempted to simulate the spectra using the pair average polarizability model (eq 1).[19] The calculations assume two slightly prolate particles with semimajor axes 25 nm, and semiminor axes 16 nm. One particle is Au, with optical properties from ref 23, and the other is AgI with optical properties taken from refs 24 and 25. The two particles form a pair along their rotational axes. The incident electric field is assumed to be polarized perpendicular to the pair axis (as is the case for the experimental spectra in Figure 3). The simulated spectra shown in Figure 6 were calculated assuming different interparticle separation distances $d_{12}$. The spectra simulated using the pair average polarizability model clearly do not describe the effects seen in the experimental spectra. As the distance between the Au and AgI segments decreases, the plasmon resonance maximum in the simulated spectra does not red-shift. Also in contrast to the experimental data, the exciton peak at the AgI band edge remains strong at all interparticle distances.

Figure 7 shows polarization spectra calculated for Au/AgI pair particles in contact. Figure 7A shows the large spectral range encompassing both short- and long-axis plasmon resonance bands. Figure 7B is a detailed view of the spectral range encompassing the AgI band edge and the Au short-axis resonance. While the simulated spectra show a increase in the

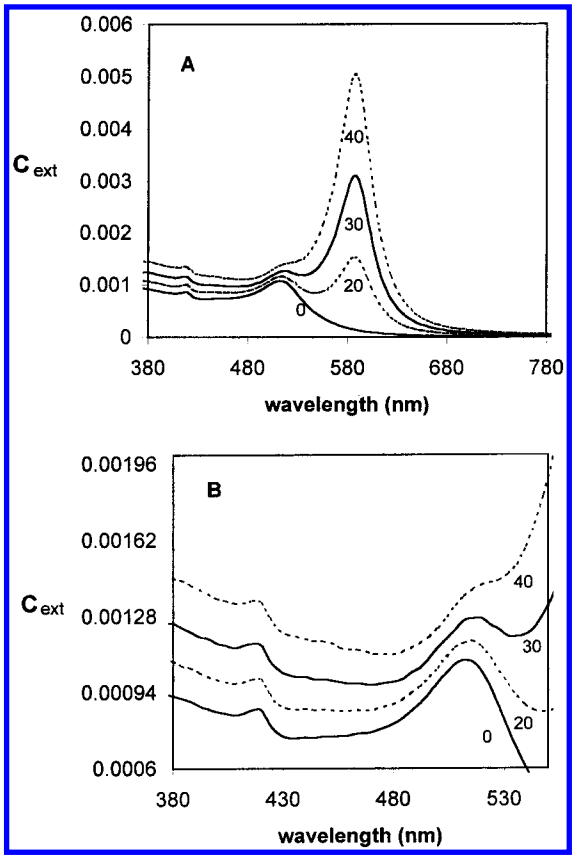


**Figure 7.** Polarization extinction spectra calculated using pair average polarizability model for contacting Au/AgI particle pairs. Particle dimensions: Au ($a$ = 38 nm; $b$ = 16 nm). AgI ($a$ = 20 nm, $b$ = 16 nm). **(**A**)** p-Polarization spectra showing short- and long-axis resonance bands. (B**)** Detail view of AgI band edge and short-axis resonance. Incidence angles given next to curves.

long-axis extinction with increasing incidence angle, the magnitude of the long-axis extinction is much larger than seen in experiment. We should also note that the position of the calculated long-axis resonance maximum ($\lambda_{max}$ = 588 nm) is insensitive to the presence of the contacting AgI particle. Spectra calculated for isolated Au particles ($a$ = 38 nm, $b$ = 16 nm) show an identical $\lambda_{max}$ value. In the experimental spectra, the long-axis resonance maximum in the Au/AgI system occurs at 730 nm, compared to 690 nm in the case of the isolated Au rods.

**Consequences of Au and AgI Mixing**. The failure of the pair average polarizability model to account for the spectral features seen in experiment (plasmon resonance shifts and exciton peak damping) led us to consider the possibility that the Au and AgI particles are not, at least in the case of ostensibly contacting phases, compositionally pure. The intermixing of metals and semiconductors at phase boundaries is a well-known problem in the electronics industry.[26,27] The mixing may occur at the nanoscale level, with many atom clusters of Au and AgI forming a random aggregate. At the other extreme, mixing may occur at the atomic level, with Au atoms diffusing into the AgI phase, and vice versa.

Figure 8 shows a series of spectra (curves 2−4) calculated using the pair-average polarizability model as before, but with the pair members themselves now being mixtures of spherical Au and AgI components. The optical constants of the composite particles were calculated using the Bruggeman effective medium treatment.[16] As the degree of mixing increases, the Au plasmon resonance band red-shifts and broadens in a manner similar to

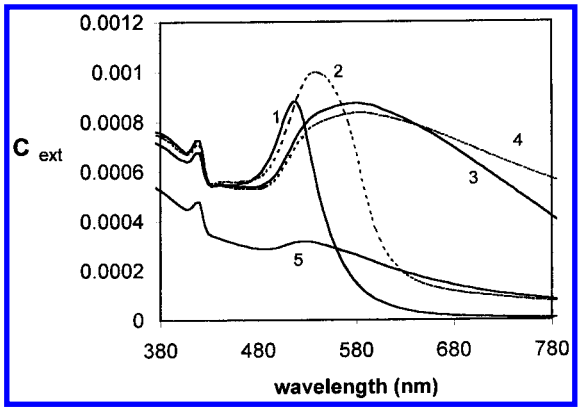


**Figure 8.** Normal incidence extinction spectra calculated using the pair average polarizability model assuming intermixing of Au and AgI phases. Dimensions of both particles $a = 25$ nm, $b = 16$ nm. Interparticle spacing $d_{12} = 50$ nm. (Curve 1) Particle 1 is pure Au, particle 2 pure AgI. (Curve 2) Particle 1 has Au volume fraction ($f_{Au}$) = 0.9, AgI volume fraction ($f_{AgI}$) = 0.1; particle 2 $f_{AgI} = 0.9$, $f_{Au} = 0.1$. (Curve 3) Particle 1 $f_{Au} = 0.7$, $f_{AgI} = 0.3$; particle 2 $f_{AgI} = 0.7$, $f_{Au} = 0.3$. (Curve 4) Both particles $f_{Au} = f_{AgI} = 0.5$. (Curve 5) Au particle possesses impurity-reduced electron mean free lifetime $6 \times 10^{-16}$ s (compared to bulk value of $9.3 \times 10^{-15}$ s).

experiment. However, in contrast to experiment, the AgI exciton peak in the calculated spectra remains strong at all compositions.

The first four curves of Figure 8 assume that the Au and AgI subdomains are large enough to possess bulk optical properties. If atomic level mixing occurs, the impurity atoms do not possess bulk optical properties, but likely act to alter the properties of their host. In the case of Ag or I atoms diffusing into the Au phase, one would expect the lattice disruption to result in a decrease in the mean free lifetime ($\tau$) of the Au conduction electrons. Curve 5 in Figure 8 shows the spectrum of an Au/AgI pair system in which the Au $\tau$ value has been reduced[27] from the bulk value of $9.3 \times 10^{-15}$ to $6 \times 10^{-16}$ s. Reducing $\tau$ has the combined effect of red-shifting and damping the Au plasmon resonance band. The plasmon band shape is quite similar to the experimental spectra. The exciton feature is unchanged because we did nothing to alter the AgI properties.

The large domain and atomic level intermixing models provide plausible explanations for the red-shifting and peak broadening of the Au plasmon resonance band. In the case of complete conversion of the second Ag layer to AgI (Figure 3, bottom curve), the intimate contact between the Au and AgI phases allows for intermixing. When a large Ag spacing layer is left unconverted and subsequently etched, the Au and AgI phases do not intermix (Figure 3, top curve). The observation of intermediate behavior (Figure 3, middle curve) suggests that there is an inherent distribution in interparticle spacing; when we attempt to introduce a very thin spacing between the Au and AgI phases, a significant fraction of the particles are actually in contact and intermixing can occur.

Contamination of the AgI phase by Au atoms or clusters may also explain the absence of the exciton peak in the spectra of contacting particles. The well-known two-particle Hamiltonian for electron−hole interaction is[28]

$$H = -\frac{\hbar^2}{2m_h}\nabla^2 - \frac{\hbar^2}{2m_e}\nabla^2 - \frac{e^2}{\epsilon_s|r_e - r_h|} \qquad (2)$$

where the first two terms on the right-hand side are the kinetic energy operators for the hole and electron, respectively, and the third term is the potential energy of the electron−hole interaction. $\epsilon_s$ is the static dielectric constant of the medium, and $r_e$ and $r_h$ are the position vectors of the electron and hole, respectively. The $\epsilon_s$ value for pure AgI is ca. 7.[29] It is reasonable to assume that the presence of Au atoms or clusters will result in an increase in the static dielectric constant, and therefore weaken the Coulombic attraction between the electron and hole.

One feature of metal−semiconductor contacts is the formation of a contact potential difference. If the resulting electric field on the semiconductor side of the junction is sufficiently large, then the dc Stark effect might be expected to cause a red shift and broadening of the exciton resonance.[28] Assuming a Bohr radius of ca. 2 nm for the AgI exciton, and a binding energy of 80 meV,[29] we estimate that a field of ca. $3 \times 10^3$ V/cm would be required to disrupt the exciton.[30] From the free carrier concentration data of Patnaik and Sunandana,[31] we estimate a space charge region thickness of ca. 0.3 $\mu$m, which is significantly larger than the AgI nanoparticles considered in this study. Thus, it is unlikely that the full 0.46 V contact potential of bulk Au/AgI systems reported by Ukshe et al.[32] is established, and it is therefore difficult to predict the electric field in the semiconductor phase of the AgI nanoparticles.[33]

Exciton disruption due to dc field induced ionization of impurities is also well-known. The free carriers liberated by such ionization increase the effective dielectric constant of the medium, and thus screen electron−hole interactions. Considering that the magnitude of the fields required are smaller (ca. 5−30 V/cm[28]), and that our electrochemical synthesis method likely engenders more impurities than vacuum based methods, the impurity ionization mechanism for exciton disruption seems quite reasonable.

The mechanisms described above require physical contact between the metal and semiconductor phases and consequent intermixing and/or establishment of an internal static field. For two particles merely in close proximity, it is possible that image interactions may lead to damping of the exciton resonance in a manner analogous to that predicted for the absorption lines of atoms near metal surfaces.[34] However, considering the effects observed for both the Au plasmon band and the AgI exciton, it would seem that metal/semiconductor intermixing is a more reasonable model. Our intial attempts to obtain elemental profiles of the nanoparticles via energy-dispersive X-ray (EDX) analysis were not fruitful.

## V. Conclusions

We have demonstrated that electrochemical template synthesis can be used to prepare metal−semiconductor nanoparticle pair structures in which the two members are, on average, either in contact or separated. The extinction spectra of the Au/AgI pair systems indicate a systematic dependence on the amount of silver left unoxidized as a spacing group between the Au and AgI. When all of the Ag in contact with the Au particle is converted to AgI, the experimental spectra show an Au plasmon resonance band that is red-shifted and broadened, and the absence of the exciton peak normally associated with the AgI band edge. When part of the deposited silver is not converted to AgI, and subsequently etched away, the Au plasmon band blue-shifts and narrows, and the AgI exciton reappears.

The observed spectral changes with decreasing average interparticle spacing are not predicted even qualitatively by a pair-average polarizability model that assumes phase purity. The red-shifting and broadening of the Au plasmon resonance band in the case of contacting particles is, however, consistent with intermixing of the metal and semiconductor components. The absence of the AgI exciton peak in the case of contacting Au and AgI phases, and its presence in systems involving large

interparticle spacing, are also consistent with phase intermixing; Au contamination of the AgI phase may act to screen electron−hole interactions. This screening may also be enhanced by field-induced impurity ionization arising from a contact potential at the Au−AgI interface.

Identifying the precise mechanism of metal−semiconductor phase interaction in the Au/AgI nanoparticle pair system will require further information on the composition of the two phases. Regardless of the mechanism, it is clear that the application of the electrochemical template synthesis method to particle structures containing more than one material is not straightforward; when nanoparticles composed of two different materials are in contact, their optical spectra do not suggest a simple average of the spectra of the two materials in their pure form.

**Acknowledgment.** This work was supported by the National Science Foundation (NSF DMR 9625151). Electron microscopy support was provided by the Lombardi Cancer Center Microscopy and Imaging Shared Resource (U.S. Public Health Grant 2P30-CA-51008).

## References and Notes

(1) Preston, C. K.; Moskovits, M. *J. Phys. Chem.* **1993**, *97*, 8405.
(2) Preston, C. K.; Moskovits, M. *J. Phys. Chem.* **1988**, *92*, 2957.
(3) Tierney, M. J.; Martin, C. R. *J. Phys. Chem.* **1989**, *93*, 2878.
(4) Foss, C. A.; Hornyak, G. L.; Stockert, J. A.; Martin, C. R. *J. Phys. Chem.* **1994**, *98*, 2963.
(5) Routkevitch, D.; Bigioni, T.; Moskovits, M.; Xu, J. M. *J. Phys. Chem. B* **1996**, *100*, 14037.
(6) Lakshimi, B. B.; Dorhout, P. K.; Martin, C. R. *Chem. Mater.* **1997**, *9*, 857.
(7) Martin, C. R. *Acc. Chem. Res.* **1995**, *28*, 61.
(8) Al-Rawashdeh, N.; Sandrock, M. L.; Seugling, C.; Foss, C. A., Jr. *J. Phys. Chem. B* **1998**, *102*, 361.
(9) Sandrock, M. L.; Pibel, C. D.; Geiger, F. M.; Foss, C. A., Jr. *J. Phys. Chem. B.* **1999**, *103*, 2668.
(10) El-Kouedi, M.; Sandrock, M. L.; Seugling, C. J.; Foss, C. A., Jr. *Chem. Mater.* **1998**, *10*, 3287.
(11) Klein, J. D.; Herrick, R. D. II, Palmer, D.; Sailor, M. J.; Brumlik, C. J.; Martin, C. R. *Chem. Mater.* **1993**, *5*, 902.
(12) Schneer, C. J.; Whiting, R. W. *Am. Mineral.* **1963**, *48*, 737.
(13) Berry, C. R. *Phys. Rev.* **1967**, *161*, 848.
(14) van de Hulst, H. C. *Light Scattering by Small Particles*; Dover: New York, 1980.
(15) Bohren, C. F.; Huffman, D. R. *Absorption and Scattering of Light by Small Particles;* Wiley: New York, 1983.
(16) Aspnes, D. E. *Thin Solid Films* **1982**, *89*, 249.
(17) Schmitt, J.; Machtle, P.; Eck, D.; Mohwald, M.; Helm, C. A. *Langmuir* **1999**, *15*, 3256.
(18) Sandrock, M. L.; Foss, C. A., Jr. *J. Phys. Chem. B* **1999**, *103*, 11398.
(19) The extinction cross section $C_{ext}$ is the sum of the losses due to absorption ($C_{abs} = k\ \mathrm{Im}\{\langle\alpha\rangle\}$) and scattering ($C_{sca} = (k^4/6\pi)|\langle\alpha\rangle|^2$). In the simulation of the polarization spectra, the total extinction as a function of $\vartheta$ is assumed to be the weighted sum of the short and long-axis extinction components via $C_{ext}(\vartheta) = C_{ext}(\vartheta{=}90)\sin^2\vartheta + C_{ext}(\vartheta{=}0)\cos^2\vartheta$, where $C_{ext}(\vartheta{=}90)$ and $C_{ext}(\vartheta{=}0)$ are calculated assuming $g = -{}^1/_4\pi$ and $g = {}^1/_2\pi$, respectively, in the $\langle\alpha\rangle$ factor.
(20) By "first order", we mean that the only effect a particle has on its neighbor is to alter the electric field that neighbor experiences. The optical constants of the particles are assumed to be the same as those of the bulk materials.
(21) Shumilova, N. A.; Zutaeva, G. V. In *Encyclopedia of Electrochemistry of Elements*; Bard A. J., Ed.; Marcel Dekker: New York, 1978; Vol. 8, p 109.
(22) Jaya, S.; Rao, P. T.; Rao, P. G. *J. Appl. Electrochem.* **1988**, *18*, 459.
(23) Johnson, P. B.; Christy, R. W. *Phys. Rev. B* **1972**, *6*, 4370.
(24) Bedikyan, L. D.; Miloslavskii, V. K.; Ageev, L. A. *Opt. Spektrosk.* **1979**, *47*, 225.
(25) Cordona, M. *Phys. Rev.* **1963**, *129*, 69.
(26) Aldao, C. M.; Weaver, J. H. In *Contacts to Semicondutors*; Brillson, L. J., Ed.; Noyes Publications: Park Ridge, NJ, 1993; Chapter 7.
(27) Rhoderick, E. H.; Williams, R. H. *Metal-Semiconductor Contacts*, 2nd ed.; Oxford University Press: Oxford, UK, 1988.
(28) Peyghambarian, N.; Koch, S.; Mysyrowicz, A. In *Introduction to Semiconductor Optics;* Holonyak, N., Ed; Prentice Hall; NJ, 1993.
(29) von der Osteen. *Landolt-Bornstien*; New Series III/22a, p 299.
(30) The ionization field is given by $E_{ion} = E_B/e\ a_{Bohr}$ (see ref 26, p 260).
(31) Patnaik, J. R.; Sunandana, C. S. *J. Phys. Chem. Solids* **1998**, *59*, 1059.
(32) Ukshe, E. A.; Malov, Y. I.; Bukun, N. G.; Mikhailova, A. M. *Sov. Electrochem.* **1988**, *24*, 671.
(33) For bulk AgI a screening length $L_D$ of 330 nm was estimated using the well-known relation $L_D^2 = \epsilon_s\epsilon_o k_B T/2e^2 n_i$, where the static dielectric constant was assumed to be 7, and the free carrier density $n_i$ is an average of the values for $\gamma$-AgI and $\beta$-AgI (ref 31).
(34) Nordlander, P. In *Laser Spectroscopy and Photochemistry on Metal Surfaces*; Dai, M. L., Ho, W., Eds.; World Scientific Publishing: Singapore, 1995; Part 1.